



**University of
Sunderland**

Elmarakbi, Ahmed, Hu, Ning and Fukunaga, Hisao (2009) Finite element simulation of delamination growth in composite materials using LS-DYNA. *Composites Science and Technology*, 69 (14). pp. 2383-2391. ISSN 0266-3538

Downloaded from: <http://sure.sunderland.ac.uk/1598/>

Usage guidelines

Please refer to the usage guidelines at <http://sure.sunderland.ac.uk/policies.html> or alternatively contact sure@sunderland.ac.uk.



Finite element simulation of delamination growth in composite materials using LS-DYNA

A.M. Elmarakbi^{a,*}, N. Hu^{b,c}, H. Fukunaga^c

^aSchool of Computing and Technology, University of Sunderland, Sunderland SR6 0DD, UK

^bDepartment of Engineering Mechanics, Chongqing University, Chongqing 400011, PR China

^cDepartment of Aerospace Engineering, Tohoku University, Sendai 980-8579, Japan

ARTICLE INFO

Article history:

Received 25 June 2008

Received in revised form 20 January 2009

Accepted 30 January 2009

Available online 10 February 2009

Keywords:

B. Delamination growth

B. Cohesive elements

C. Finite element analysis

C. Quasi-static and dynamic analysis

ABSTRACT

In this paper, a modified adaptive cohesive element is presented. The new elements are developed and implemented in LS-DYNA, as a user defined material subroutine (UMAT), to stabilize the finite element simulations of delamination propagation in composite laminates under transverse loads. In this model, a pre-softening zone is proposed ahead of the existing softening zone. In this pre-softening zone, the initial stiffness and the interface strength are gradually decreased. The onset displacement corresponding to the onset damage is not changed in the proposed model. In addition, the critical energy release rate of the materials is kept constant. Moreover, the constitutive equation of the new cohesive model is developed to be dependent on the opening velocity of the displacement jump. The traction based model includes a cohesive zone viscosity parameter (η) to vary the degree of rate dependence and to adjust the maximum traction. The numerical simulation results of DCB in Mode-I is presented to illustrate the validity of the new model. It is shown that the proposed model brings stable simulations, overcoming the numerical instability and can be widely used in quasi-static, dynamic and impact problems.

© 2009 Elsevier Ltd. All rights reserved.

1. Introduction

Delamination is a mode of failure of laminated composite materials when subjected to transverse loads. It can cause a significant reduction in the compressive load-carrying capacity of a structure. Cohesive elements are widely used, in both forms of continuous interface elements and point cohesive elements [1–7], at the interface between solid finite elements to predict and to understand the damage behaviour in the interfaces of different layers in composite laminates. Many models have been introduced including: perfectly plastic, linear softening, progressive softening, and regressive softening [8]. Several rate-dependent models have also been introduced [9–13]. A rate-dependent cohesive zone model was first introduced by Glennie [9], where the traction in the cohesive zone is a function of the crack opening displacement time derivative. Xu et al. [10] extended this model by adding a linearly decaying damage law. In each model the viscosity parameter (η) is used to vary the degree of rate dependence. Kubair et al. [11] thoroughly summarized the evolution of these rate-dependant models and provided the solution to the mode III steady-state crack growth problem as well as spontaneous propagation conditions.

A main advantage of the use of cohesive elements is the capability to predict both onset and propagation of delamination without

previous knowledge of the crack location and propagation direction. However, when using cohesive elements to simulate interface damage propagations, such as delamination propagation, there are two main problems. The first one is the numerical instability problem as pointed out by Mi et al. [14], Goncalves et al. [15], Gao and Bower [16] and Hu et al. [17]. This problem is caused by a well-known elastic snap-back instability, which occurs just after the stress reaches the peak strength of the interface. Especially for those interfaces with high strength and high initial stiffness, this problem becomes more obvious when using comparatively coarse meshes [17]. Traditionally, this problem can be controlled using some direct techniques. For instance, a very fine mesh can alleviate this numerical instability, however, which leads to very high computational cost. Also, very low interface strength and the initial interface stiffness in the whole cohesive area can partially remove this convergence problem, which, however, lead to the lower slope of loading history in the loading stage before the happening of damages. Furthermore, various generally oriented methodologies can be used to remove this numerical instability, e.g. Riks method [18] which can follow the equilibrium path after instability. Also, Gustafson and Waas [19] have used a discrete cohesive zone method finite element to evaluate traction law efficiency and robustness in predicting decohesion in a finite element model. They provided a sinusoidal traction law which found to be robust and efficient due to the elimination of the stiffness discontinuities associated with the generalized trapezoidal traction law.

* Corresponding author.

E-mail address: ahmed.elmarakbi@sunderland.ac.uk (A.M. Elmarakbi).

Recently, the artificial damping method with additional energy dissipations has been proposed by Gao and Bower [16]. Also, the present authors proposed a kind of move-limit method [17] to remove the numerical instability using cohesive model for delamination propagation. In this technique, the move-limit in the cohesive zone provided by artificial rigid walls is built up to restrict the displacement increments of nodes in the cohesive zone of laminates after delaminations occurred. Therefore, similar to the artificial damping method [16], the move-limit method introduces the artificial external work to stabilize the computational process. As shown later, although these methods [16,17] can remove the numerical instability when using comparatively coarse meshes, the second problem occurs, which is the error of peak load in the load–displacement curve. The numerical peak load is usually higher than the real one as observed by Goncalves et al. [15] and Hu et al. [17].

Similar work has also been conducted by De Xie and Waas [20]. They have implemented discrete cohesive zone model (DCZM) using the finite element (FE) method to simulate fracture initiation and subsequent growth when material non-linear effects are significant. In their work, they used the nodal forces of the rod elements to remove the mesh size effect, dealt with a 2D study and did not consider viscosity parameter. However, in the presented paper, the authors used the interface stiffness and strength in a continuum element, tackled a full 3D study and considered the viscosity parameter in their model.

With the previous background in mind, the objective of this paper is to propose a new cohesive model named as adaptive cohesive model (ACM), for stably and accurately simulating delamination propagations in composite laminates under transverse loads. In this model, a pre-softening zone is proposed ahead of the existing softening zone. In this pre-softening zone, with the increase of effective relative displacements at the integration points of cohesive elements on interfaces, the initial stiffnesses and interface strengths at these points are reduced gradually. However, the onset displacement for starting the real softening process is not changed in this model. The critical energy release rate or fracture toughness of materials for determining the final displacement of complete decohesion is kept constant. Also, the traction based model includes a cohesive zone viscosity parameter (η) to vary the degree of rate dependence and to adjust the peak or maximum traction.

In this paper, this cohesive model is formulated and implemented in LS-DYNA [21] as a user defined materials (UMAT). LS-DYNA is one of the explicit FE codes most widely used by the automobile and aerospace industries. It has a large library of material options; however, continuous cohesive elements are not available within the code. The formulation of this model is fully three-dimensional and can simulate mixed-mode delamination. However, the objective of this study is to develop new adaptive cohesive elements able to capture delamination onset and growth under quasi-static and dynamic Mode-I loading conditions. The capabilities of the proposed elements are proven by comparing the numerical simulations and the experimental results of DCB in Mode-I.

2. The constitutive model

Cohesive elements are used to model the interface between sublaminates. The elements consists of a near zero-thickness volumetric element in which the interpolation shape functions for the top and bottom faces are compatible with the kinematics of the elements that are being connected to it [22]. Cohesive elements are typically formulated in terms of traction vs. relative displacement relationship. In order to predict the initiation and growth

of delamination, an 8-node cohesive element shown in Fig. 1 is developed to overcome the numerical instabilities.

The need for an appropriate constitutive equation in the formulation of the interface element is fundamental for an accurate simulation of the interlaminar cracking process. A constitutive equation is used to relate the traction to the relative displacement at the interface. The bilinear model, as shown in Fig. 2, is the simplest model to be used among many strain softening models. Moreover, it has been successfully used by several authors in implicit analyses [23–26]. However, using the bilinear model leads to numerical instabilities in an explicit implementation. To overcome this numerical instability, a new adaptive model is proposed and presented in this paper.

The adaptive interfacial constitutive response shown in Fig. 3 is implemented as follows:

- 1. In pre-softening zone, $\alpha\delta_m^o < \delta_m^{max} < \delta_m^o$, the constitutive equation is given by

$$\sigma = (\sigma_m + \eta\dot{\delta}_m) \frac{\delta_m}{\delta_m^o} \tag{1}$$

$$\text{and } \sigma_m = K\delta_m^o \tag{2}$$

where σ is the traction, K is the penalty stiffness and can be written as

$$K = \begin{cases} K_o & \delta_m \leq 0 \\ K_i & \delta_m^{max} < \delta_m^o \\ K_n & \delta_m^o \leq \delta_m^{max} < \delta_m^f \end{cases} \tag{3}$$

δ_m is the relative displacement in the interface between the top and bottom surfaces (in this study, it equals the normal relative displacement for Mode-I), δ_m^o is the onset displacement and it is remained constant in the simulation and can be determined as follows:

$$\delta_m^o = \frac{\sigma_o}{K_o} = \frac{\sigma_i}{K_i} = \frac{\sigma_{min}}{K_{min}} \tag{4}$$

where σ_o is the initial interface strength, σ_i is the updated interface strength in the pre-softening zone, σ_{min} is the minimum limit of the

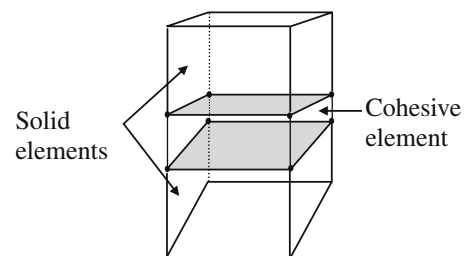


Fig. 1. Eight-node cohesive element.

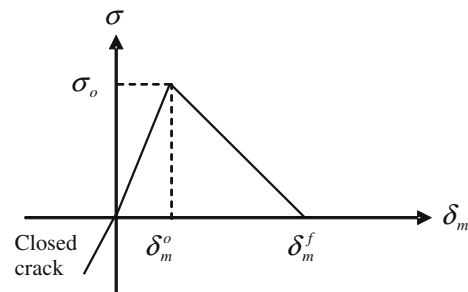


Fig. 2. Normal (bilinear) constitutive model.

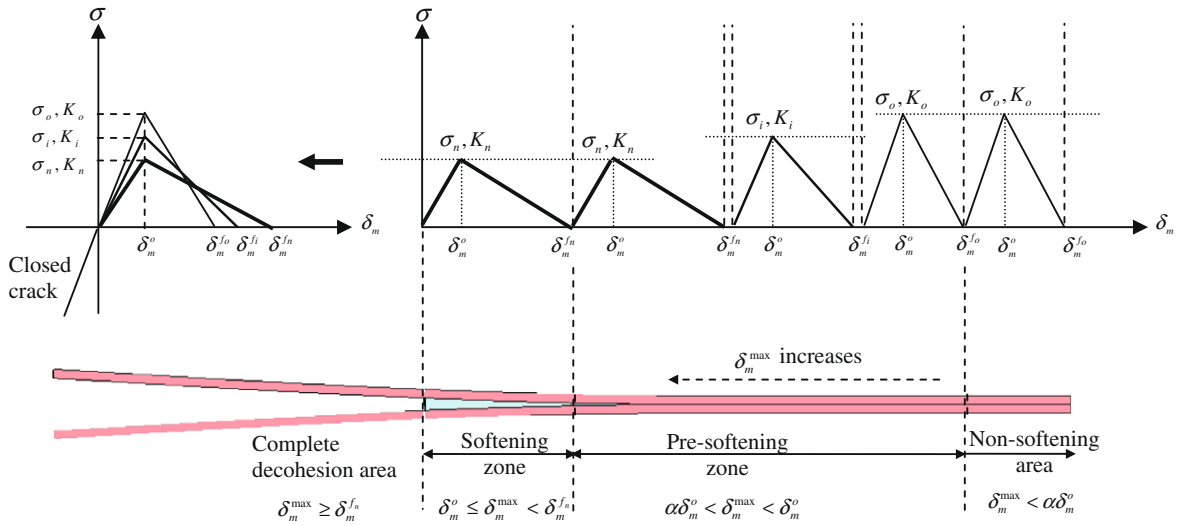


Fig. 3. Adaptive constitutive model for Mode-I.

interface strength, K_o is the initial stiffness, K_i is the updated stiffness in the pre-softening zone, and K_{min} is the minimum value of the stiffness.

For each increment and for time $t + 1$, δ_m is updated as follows:

$$\delta_m^{t+1} = t_c \varepsilon^{t+1} - t_c \quad (5)$$

where t_c is the thickness of the cohesive element and ε^{t+1} is the normal strain of the cohesive element for time $t + 1$, $\varepsilon^{t+1} = \varepsilon^t + \Delta\varepsilon$, where $\Delta\varepsilon$ is the normal strain increment.

The $(\delta_m^{max})^t$ is the max relative displacement of the cohesive element occurs in the deformation history. For each increment and for time $t + 1$, δ_m^{max} is updated as follows:

$$(\delta_m^{max})^{t+1} = \delta_m^{t+1} \quad \text{if } \delta_m^{t+1} \geq (\delta_m^{max})^t \quad \text{and,} \quad (6)$$

$$(\delta_m^{max})^{t+1} = (\delta_m^{max})^t \quad \text{if } \delta_m^{t+1} < (\delta_m^{max})^t \quad (7)$$

Using the max value of the relative displacement δ_m^{max} rather than the current value δ_m prevents healing of the interface. The updated stiffness and interface strength are determined in the following forms:

$$\sigma_i = \frac{\delta_m^{max}}{\delta_m^o} (\sigma_{min} - \sigma_o) + \sigma_o, \quad \sigma_o > \sigma_{min} \quad \text{and} \quad (\alpha \delta_m^o < \delta_m^{max} < \delta_m^o) \quad (8)$$

$$K_i = \frac{\delta_m^{max}}{\delta_m^o} (K_{min} - K_o) + K_o, \quad (K_o > K_{min} \quad \text{and} \quad (\alpha \delta_m^o < \delta_m^{max} < \delta_m^o)) \quad (9)$$

It should be noted that α in Eqs. (8) and (9) is a parameter to define the size of pre-softening zone. When $\alpha = 1$, the present adaptive cohesive mode degenerates into the traditional cohesive model.

In our computations, we set $\alpha = 0$. From our numerical experiences, the size of pre-softening zone has some influences on the initial stiffness of loading–displacement curves, but not so significant. The reason is that for the region far always from the crack tip, the interface decrease or update according to Eqs. (8) and (9) is not obvious since δ_m^{max} is very small.

The energy release rate for Mode-I G_{IC} also remains constant. Therefore, the final displacements associated to the complete decohesion δ_m^f are adjusted as shown in Fig. 3 as

$$\delta_m^f = \frac{2G_{IC}}{\sigma_i} \quad (10)$$

Once the max relative displacement of an element located at the crack front satisfies the following conditions; $\delta_m^{max} > \delta_m^o$, this ele-

ment enters into the real softening process. Where, as shown in Fig. 3, the real softening process denotes a stiffness decreasing process caused by accumulated damages. Then, the current strength σ_n and stiffness K_n , which are almost equal to σ_{min} and K_{min} , respectively, will be used in the softening zone.

2. In softening zone, $\delta_m^o \leq \delta_m^{max} < \delta_m^f$, the constitutive equation is given by

$$\sigma = (1 - d)(\sigma_m + \eta \dot{\delta}_m) \frac{\delta_m}{\delta_m^o} \quad (11)$$

where d is the damage variable and can be defined as

$$d = \frac{\delta_m^f (\delta_m^{max} - \delta_m^o)}{\delta_m^{max} (\delta_m^f - \delta_m^o)}, \quad d \in [0, 1] \quad (12)$$

The above adaptive cohesive mode is of the engineering meaning when using coarse meshes for complex composite structures, which is, in fact, an ‘artificial’ means for achieving the stable numerical simulation process. A reasonable explanation is that all numerical techniques are artificial, whose accuracy strongly depends on their mesh sizes, especially at the front of crack tip. To remove the factitious errors in the simulation results caused by the coarse mesh sizes in the numerical techniques, we artificially adjust some material properties in order to partially alleviate or remove the numerical errors. Otherwise, we have to resort very fine meshes, which may be computationally impractical for very complex problems from the capabilities of most current computers. Of course, the modified material parameters should be those which do not have the dominant influences on the physical phenomena. For example, the interface strength usually controls the initiation of interface cracks. However, it is not crucial for determining the crack propagation process and final crack size from the viewpoint of fracture mechanics. Moreover, there has been almost no clear rule to exactly determine the interface stiffness, which is a parameter determined with a high degree of freedom in practical cases. Therefore, the effect of the modifications of interface strength and stiffness can be very small since the practically used onset displacement δ_m^o for delamination initiation is remained constant in our model. For the parameters, which dominate the fracture phenomena, should be unchanged. For instance, in our model, the fracture toughness dominating the behaviors of interface damages is kept constant.

3. Finite element implementation

The proposed cohesive element is implemented in LS-DYNA finite element code as a user defined material (UMAT) using the standard library 8-node solid brick element. This approach for the implementation requires modelling the resin rich layer as a non-zero thickness medium. In fact, this layer has a finite thickness and the volume associated with the cohesive element can in fact set to be very small by using a very small thickness (e.g. 0.01 mm). To verify these procedures, the crack growth along the interface of a double cantilever beam (DCB) is studied. The two arms are modelled using standard LS-DYNA 8-node solid brick elements and the interface elements are developed in a FORTRAN subroutine using the algorithm shown in Fig. 4.

The LS-DYNA code calculates the strain increments for a time step and passes them to the UMAT subroutine at the beginning of each time step. The material constants, such as the stiffness and strength, are read from the LS-DYNA input file by the subroutine. The current and maximum relative displacements are saved as history variables which can be read in by the subroutine. Using the history variables, material constants, and strain increments, the subroutine is able to calculate the stresses at the end of the time step by using the constitutive equations. The subroutine then updates and saves the history variables for use in the next time

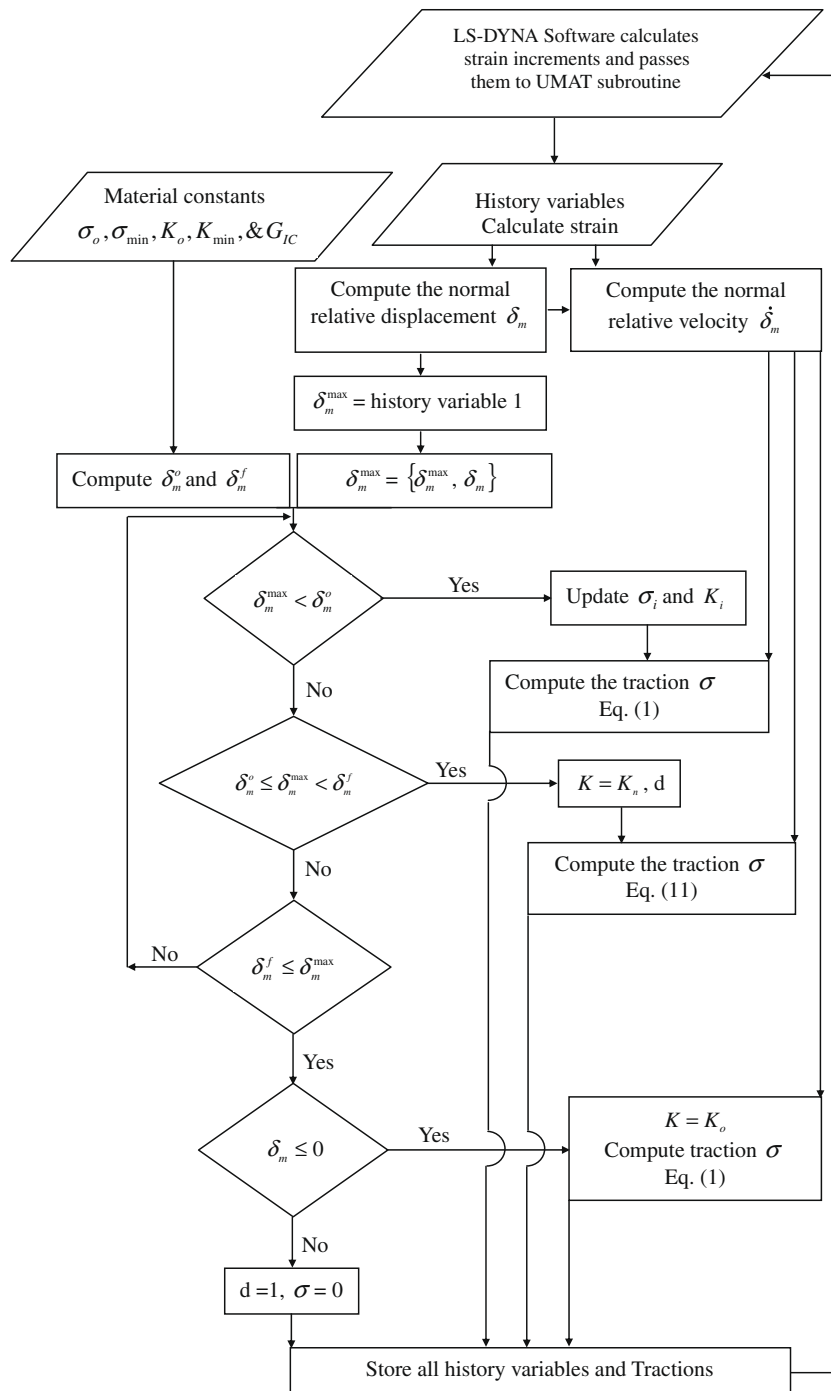


Fig. 4. Flow chart for traction computation in Mode-I.

step and outputs the calculated stresses. Note that the *DATA-BASE_EXTENT_BINARY command is required to specify the storage of history variables in the output file.

It is worth noting that the stable explicit time step is inversely proportional to the maximum natural frequency in the analysis. The small thickness elements drive up the highest natural frequency, therefore, it drives down the stable time step. Hence, mass scaling is used to obtain faster solutions by achieving a larger explicit time step when applying the cohesive element to quasi-static situations. Note that the volume associated with the cohesive element would be small by using a small thickness and the element's kinetic energy arising from this be still several orders of magnitude below its internal energy, which is an important consideration for quasi-static analyses to minimize the inertial effects.

4. Numerical simulations

4.1. Quasi-static analysis

The DCB specimen is made of a unidirectional fibre-reinforced laminate containing a thin insert at the mid-plane near the loaded end. A 150 mm long specimen (L), 20 mm wide (w) and composed of two thick plies of unidirectional material ($2h = 2 \times 1.98$ mm) shown in Fig. 5 was tested by Morais [27]. The initial crack length (l_c) is 55 mm. A displacement rate of 10 mm/s is applied to the appropriate points of the model. The properties of both carbon fibre-reinforced epoxy material and the interface are given in Table 1.

The LS-DYNA finite element model, which is shown deformed in Fig. 6, consists of two layers of fully integrated S/R 8-noded solid elements, with three elements across the thickness. Two cases with different mesh sizes are used in the initial analysis, namely: Case A, which includes eight elements across the width, and Case B, which includes one element across the width, respectively. The two cases are compared using the new cohesive elements with mesh size of 1 mm to figure out the anticlastic effects.

A plot of a reaction force as a function of the applied end displacement is shown in Fig. 7. It is clearly shown that both cases bring similar results with peak load value of 64 N. Therefore, the anticlastic effects are neglected and only one element (Case B) is used across the width in the following analyses.

Different cases are considered in this study and given in Table 2 to investigate the influence of the new adaptive cohesive element

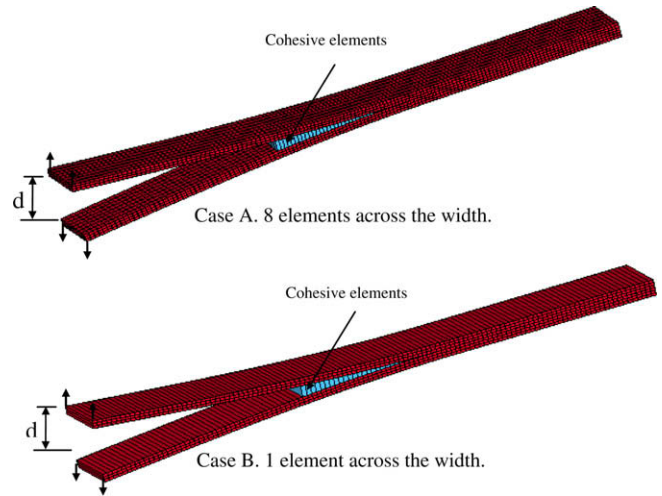


Fig. 6. LS-DYNA finite element model of the deformed DCB specimen.

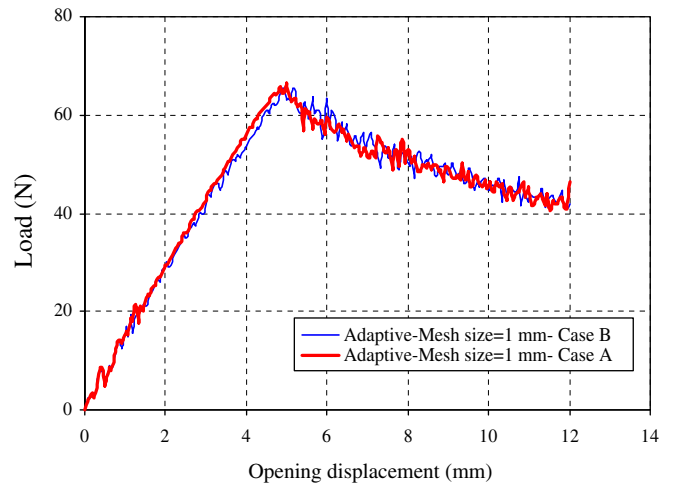


Fig. 7. Load–displacement curves for a DCB specimen in both Cases A and B.

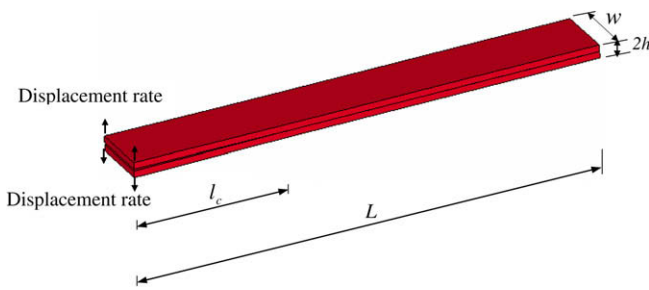


Fig. 5. Model of DCB specimen.

Table 1
Properties of both carbon fibre-reinforced epoxy material and specimen interface.

Carbon fibre-reinforced epoxy material	DCB specimen interface
$\rho = 1444 \text{ kg/m}^3$	$G_{IC} = 0.378 \text{ kJ/m}^2$
$E_{11} = 150 \text{ GPa}, E_{22} = E_{33} = 11 \text{ GPa}$	$K_o = 3 \times 10^4 \text{ N/mm}^3$
$\nu_{12} = \nu_{13} = 0.25, \nu_{23} = 0.45$	$\sigma_o = 45 \text{ MPa}$ Case I
$G_{12} = G_{13} = 6.0 \text{ MPa}, G_{23} = 3.7 \text{ MPa}$	$\sigma_o = 60 \text{ MPa}$ Case II

using different mesh sizes. The aim of the first five cases is to study the effect of the element size with constant values of interface strength and stiffness on the load–displacement relationship. Different element sizes are used along the interface spanning from very small size of 0.5 mm to coarse mesh of 2 mm. Moreover, Cases 3, 6, and 7 are to study the effect of the value of minimum interface strength on the results. Finally, Cases 6 and 8 are to find out the effect of the high interfacial strength.

Figs. 8 and 9 show the load–displacement curves for both normal (bilinear) and adaptive cohesive elements in Cases 1 and 5, respectively, with different element sizes. Fig. 8 clearly shows that the bilinear formulation results in a severe instability once the crack starts propagating. However, the adaptive constitutive law is able to model the smooth, progressive crack propagation. It is worth mentioning that the bilinear formulation brings smooth results by decreasing the element size. And it is clearly noticeable from Fig. 9 that both bilinear and adaptive formulations are found to be stable in Case 5 with very small element size. This indicates that elements with very small sizes need to be used in the softening zone to obtain high accuracy using bilinear formulation. However, this leads to large computational costs compare to Case 1. On the other hand, Fig. 10, which presents the load–displacement curves, obtained with the use of the adaptive formulation in the first five cases, show a great agreement of the results regardless

Table 2
Different cases of analyses.

Case 1	Mesh size = 2 mm	$\sigma_o = 45 \text{ MPa}, \sigma_{\min} = 15 \text{ MPa}$	$K_o = 3 \times 10^4 \text{ N/mm}^3, K_{\min} = 1 \times 10^4 \text{ N/mm}^3$
Case 2	Mesh size = 1.25 mm		
Case 3	Mesh size = 1 mm		
Case 4	Mesh size = 0.75 mm	$\sigma_o = 45 \text{ MPa}, \sigma_{\min} = 22.5 \text{ MPa}$	$K_o = 3 \times 10^4 \text{ N/mm}^3, K_{\min} = 1.5 \times 10^4 \text{ N/mm}^3$
Case 5	Mesh size = 0.5 mm		
Case 6	Mesh size = 1 mm		
Case 7	Mesh size = 1 mm		
Case 8	Mesh size = 1 mm		
		$\sigma_o = 45 \text{ MPa}, \sigma_{\min} = 10 \text{ MPa}$	$K_o = 3 \times 10^4 \text{ N/mm}^3, K_{\min} = 0.667 \times 10^4 \text{ N/mm}^3$
		$\sigma_o = 60 \text{ MPa}, \sigma_{\min} = 30 \text{ MPa}$	$K_o = 3 \times 10^4 \text{ N/mm}^3, K_{\min} = 1.5 \times 10^4 \text{ N/mm}^3$

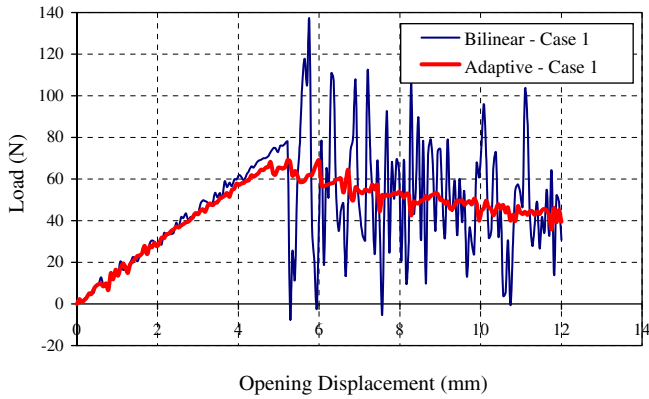


Fig. 8. Load–displacement curves obtained using both bilinear and adaptive formulations – Case 1.

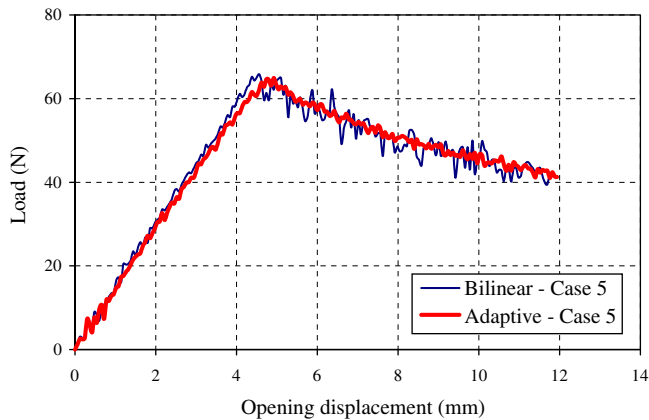


Fig. 9. Load–displacement curves obtained using both bilinear and adaptive formulations – Case 5.

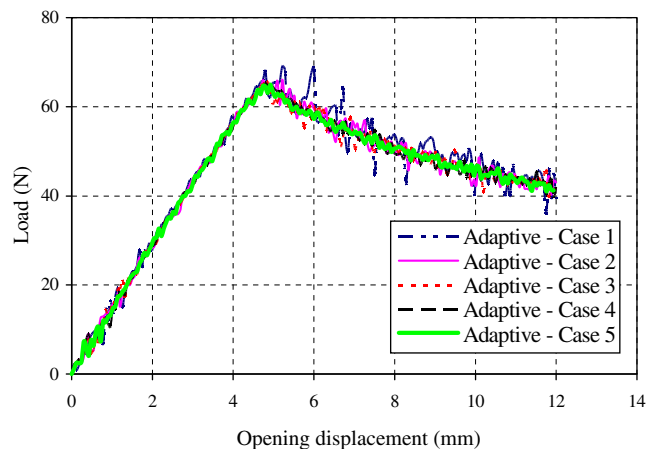


Fig. 10. Load–displacement curves obtained using the adaptive formulation – Cases 1–5.

the mesh size. Adaptive cohesive model (ACM) can yield very good results from the aspects of the peak load and the slope of loading curve if σ_{\min} is properly defined. From this figure, it can be found that the different mesh sizes result in almost the same loading curves. Even, with 2 mm mesh size, which considerable large size, although the oscillation is higher compared with those of fine mesh size, ACM still models the propagation in stable manner. The oscillation of the curve once the crack starts propagates became less by decreasing the mesh size. Therefore, the new adaptive model can be used with considerably larger mesh size and the computational cost will be greatly minimized.

The load–displacement curves obtained from the numerical simulation of Cases 3, 6 and 7 are presented in Fig. 11 together with experimental data [28]. It can be seen that the average maximum load obtained in the experiments is 62.5 N, whereas the average maximum load predicted from the three cases is 65 N. It can be observed that numerical curves slightly overestimate the load. It is worth noting that with the decrease of interface strength, the result is stable, very good result can be obtained by comparing with the experimental ones, however, the slope of loading curve before the peak load is obviously lower than those of experimental ones (Case 7; $\sigma_{\min} = 10.0 \text{ MPa}$). In Case 6 ($\sigma_{\min} = 22.5 \text{ MPa}$) and Case 3 ($\sigma_{\min} = 15 \text{ MPa}$), excellent agreements between the experimental data and the numerical predictions is obtained although the oscillation in Case 6 is higher compared with those of Case 3. Also, the slope of loading curve in Case 3 is closer to the experimental results compared with that in Case 6.

Fig. 12 show the load–displacement curves of the numerical simulations obtained using the bilinear formulation in both cases, i.e., Cases 6 and 8. The bilinear formulations results in a severe instabilities once the crack starts propagation. It is also shown that a higher maximum traction (Case 8) resulted in a more severe instability compared to a lower maximum traction (Case 6). However, as shown in Fig. 13, the load–displacement curves of the numerical simulations obtained using the adaptive formulations

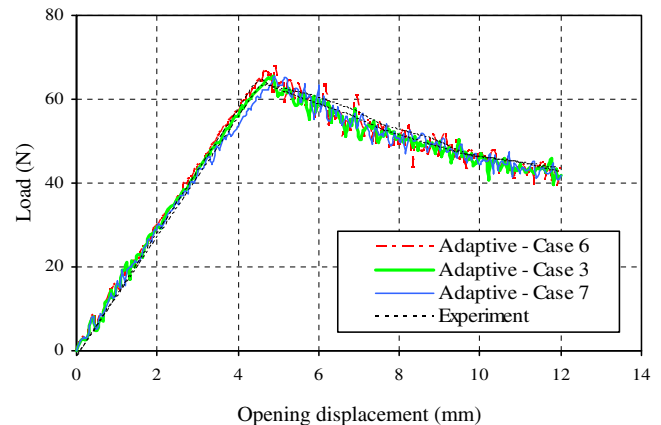


Fig. 11. Comparison of experimental and numerical simulations using the adaptive formulation – Cases 3, 6 and 7.

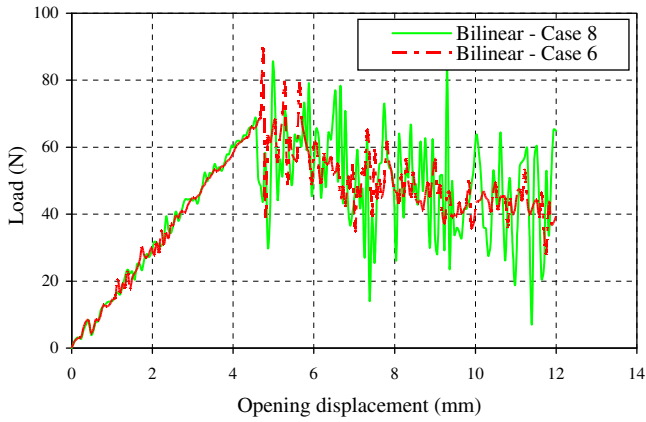


Fig. 12. Load–displacement curves obtained using the bilinear formulation – Cases 6 and 8.

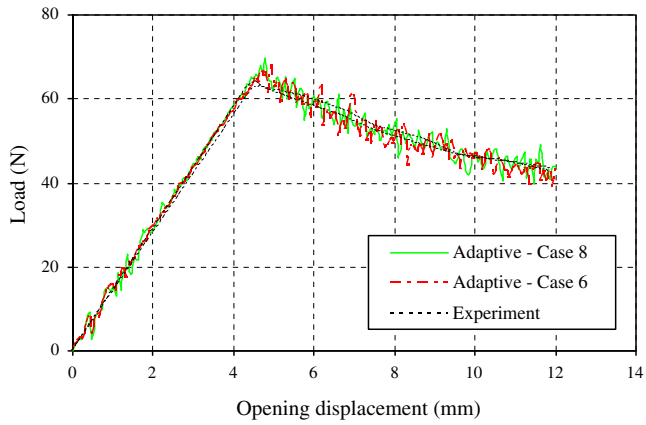


Fig. 13. Comparison of experimental and numerical simulations using the adaptive formulation – Cases 6 and 8.

are very similar in both cases. The maximum load obtained from Case 8 is found to be 69 N while in Case 6, the maximum load obtained is 66 N. The adaptive formulation is able to model the smooth, progressive crack propagation and also to produce close results compared with the experimental ones.

4.2. Dynamic analysis

The DCB specimen, as shown in Fig. 5, is made of an isotropic fibre-reinforced laminate containing a thin insert at the mid-plane near the loaded end, $L = 250$ mm, $w = 25$ mm and $h = 1.5$ mm, was analyzed by Moshier [29]. The initial crack length (l_c) is 34 mm. A displacement rate of 650 mm/s is applied to the appropriate points of the model. Young’s modulus, density and Poisson’s ratio of carbon fibre-reinforced epoxy material are given as $E = 115$ GPa, $\rho = 1566$ Kg/m³, and $\nu = 0.27$, respectively. The properties of the DCB specimen interface are given as following:

$$G_{IC} = 0.7 \text{ kJ/m}^2, K_o = 1 \times 10^5 \text{ N/mm}^3, \\ K_{min} = 0.333 \times 10^5 \text{ N/mm}^3, \sigma_o = 50 \text{ MPa}, \text{ and } \sigma_{min} = 16.67 \text{ MPa}.$$

Similarly, the LS-DYNA finite element model consists of two layers of fully integrated S/R 8-noded solid elements, with three elements across the thickness.

The adaptive rate-dependent cohesive zone model is implemented using a user defined cohesive material model in LS-DYNA. Two different values of viscosity parameter are used in the simulations; $\eta = 0.01$ and 1.0 N s/mm^3 , respectively. Note that η is a mate-

rial parameter depending on deformation rate, which appears in Eqs. (1) and (11). When $\eta = 0$, it would be a traditional model without rate dependence. By observing Eq. (1), η determines the ratio between viscosity stress $\eta \dot{\delta}_m$ and interface strength σ_m since $\sigma_m = \sigma_i$ if we consider Eqs. (1) and (4) by setting $K = K_i$. For example, if we assume $\dot{\delta}_m = 6.5 \text{ mm/s}$ on the interface here (i.e., 1% of loading rate). $\eta = 0.01 \text{ N s/mm}^3$ corresponds to a low viscosity stress of 0.065 MPa, which is much lower than the initial interface strength of 50 MPa. However, $\eta = 1.0 \text{ N s/mm}^3$ corresponds to a viscosity stress of 6.5 MPa, which is around 13% of the interface strength, and denotes a higher rate dependence. In addition, two sets of simulations are performed here. The first set involves simulations of normal (bilinear) cohesive model. The second set involves simulations of the new adaptive rate-dependent model.

A plot of a reaction force as a function of the applied end displacement of the DCB specimen using cohesive elements with viscosity value of 0.01 N s/mm^3 is shown in Fig. 14. It is clearly shown from Fig. 14 that the bilinear formulation results in a severe instability once the crack starts propagating. However, the adaptive constitutive law is able to model the smooth, progressive crack propagation. It is worth mentioning that the bilinear formulation might bring smooth results by decreasing the element size.

The load–displacement curves obtained from the numerical simulation of both bilinear and adaptive cohesive model using viscosity parameter of 1.0 N s/mm^3 is presented in Fig. 15. It can be seen that, again, the adaptive constitutive law is able to model the smooth, progressive crack propagation while the bilinear for-

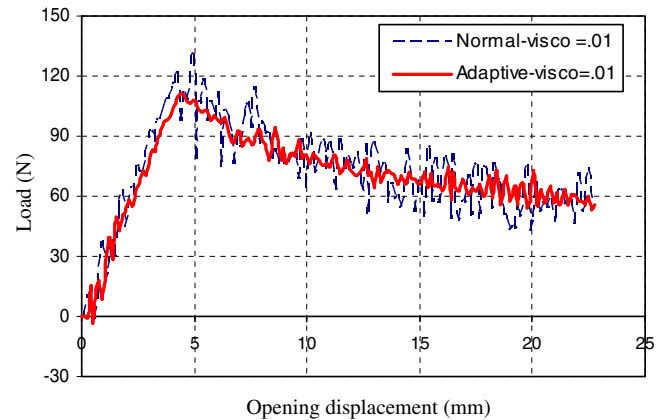


Fig. 14. Load–displacement curves obtained using both bilinear and adaptive formulations ($\eta = 0.01$).

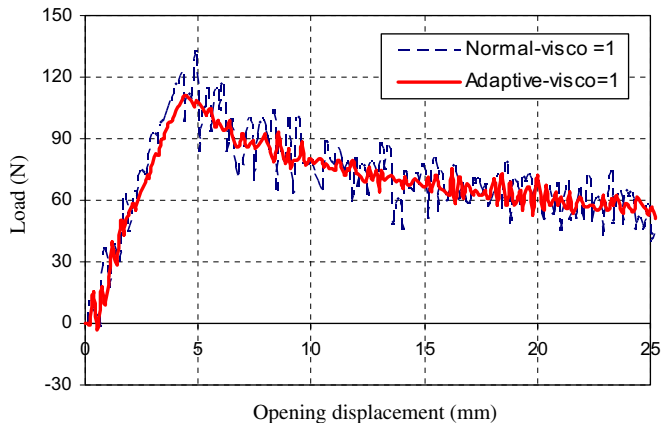


Fig. 15. Load–displacement curves obtained using both bilinear and adaptive formulations ($\eta = 1$).

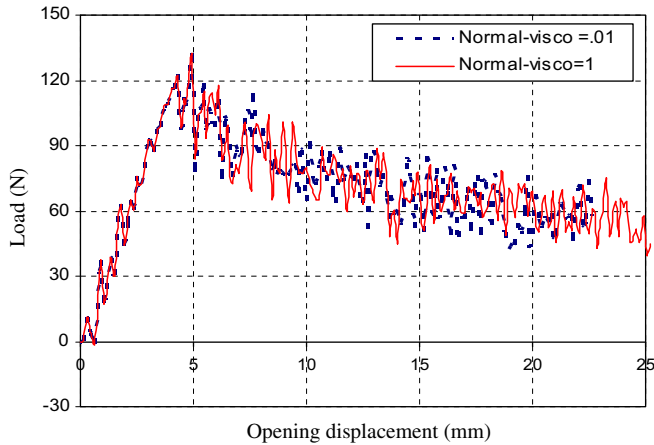


Fig. 16. Load–displacement curves obtained using bilinear formulations ($\eta = 0.01, 1$).

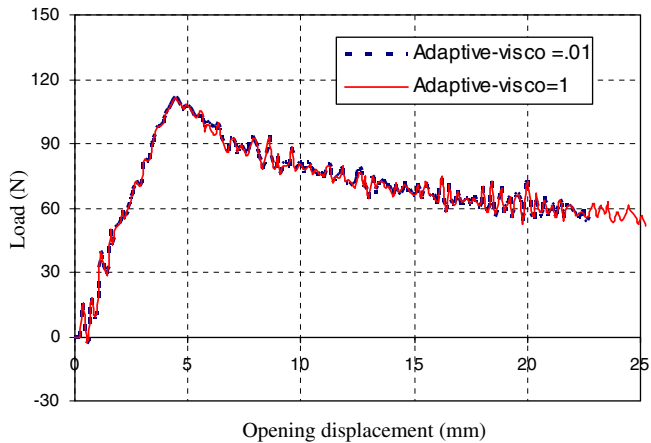


Fig. 17. Load–displacement curves obtained using adaptive formulations ($\eta = 0.01, 1$).

mulation results in a severe instability once the crack starts propagating. The average maximum load obtained using the adaptive rate-dependent model is 110 N, whereas the average maximum load predicted from the bilinear model is 120 N.

Fig. 16 shows the load–displacement curves of the numerical simulations obtained using the bilinear formulation with two different viscosity parameters, 0.01 and 1.0 N s/mm³, respectively. It is noticed from Fig. 16 that, in both cases, the bilinear formulation results in severe instabilities once the crack starts propagation. There is a very slight improvement to model the smooth, progressive crack propagation using bilinear formulations with a high viscosity parameter. On the other hand, the load–displacement curves of the numerical simulations obtained using the new adaptive formulation with two different viscosity parameters, 0.01 and 1.0 N s/mm³, respectively, is depicted in Fig. 17.

It is clear from Fig. 17 that the adaptive formulation able to model the smooth, progressive crack propagation irrespective the value of the viscosity parameter. More parametric studies will be performed in the ongoing research to accurately predict the effect of very high value of viscosity parameter on the results using both bilinear and adaptive cohesive element formulations.

5. Conclusions

A new adaptive cohesive element is developed and implemented in LS-DYNA to overcome the numerical insatiability

occurred using the bilinear cohesive model. The formulation is fully three-dimensional, and can be simulating mixed-mode delamination, however, in this study, only DCB test in Mode-I is used as a reference to validate the numerical simulations. Quasi-static and dynamic analyses are carried out in this research to study the effect of the new constitutive model. Numerical simulations showed that the new model is able to model the smooth, progressive crack propagation. Furthermore, the new model can be effectively used in a range of different element size (reasonably coarse mesh) and can save a large amount of computation. The capability of the new mode is proved by the great agreement obtained between the numerical simulations and the experimental results.

Acknowledgement

The authors wish to acknowledge the financial support provided for this ongoing research by Japan Society for the Promotion of Science (JSPS) to A.M.E. and Research Fund for Overseas Chinese Young Scholars from National Natural Science Foundation of China (No. 50728504) to N.H.

References

- [1] Camanho P, Davila C, Ambur D. Numerical simulation of delamination growth in composite materials. NASA-TP-211041; 2001: 1–19.
- [2] de Moura M, Goncalves J, Marques A, de Castro P. Modeling compression failure after low velocity impact on laminated composites using interface elements. *J Composites Mater* 1997;31:1462–79.
- [3] Reddy EJ, Mello F, Guess T. Modeling the initiation and growth of delaminations in composite structures. *J Composites Mater* 1997;31:812–31.
- [4] Chen J, Crisfield M, Kinloch A, Busso E, Matthews F, Qiu Y. Predicting progressive delamination of composite material specimens via interface elements. *Mech Composites Mater Struct* 1999;6:301–17.
- [5] Petrossian Z, Wisnom M. Prediction of delamination initiation and growth from discontinuous plies using interface elements. *Composites A* 1998;29:503–15.
- [6] Cui W, Wisnom M. A combined stress-based and fracture mechanics-based model for predicting delamination in composites. *Composites* 1993;24:467–74.
- [7] Shahwan K, Waas A. Non-self-similar decohesion along a finite interface of unilaterally constrained delaminations. In: *Proceeding of the Royal Society of London*; 1997. p. 515–50.
- [8] Camanho P, Davila C. Fracture analysis of composite co-cured structural joints using decohesion elements. *Fatigue Fract Eng Mater Struct* 2004;27:745–57.
- [9] Glennie E. A strain-rate dependent crack model. *J Mech Phys Solids* 1971;19:255–72.
- [10] Xu D, Hui E, Kramer E, Creton C. A micromechanical model of crack growth along polymer interfaces. *Mech Mater* 1991;11:257–68.
- [11] Kubair D, Geubelle P, Huang Y. Analysis of a rate dependent cohesive model for dynamic crack propagation. *Eng Fract Mech* 2003;70:685–704.
- [12] Tvergaard V, Hutchinson J. Effect of strain-dependent cohesive zone model on predictions of crack growth resistance. *Int J Solids Struct* 1996;33(20–22):3297–308.
- [13] Costanzo F, Walton J. A study of dynamic crack growth in elastic materials using a cohesive zone model. *Int J Eng Sci* 1997;35(12/13):1085–114.
- [14] Mi Y, Crisfield M, Davis G. Progressive delamination using interface element. *J Composites Mater* 1998;32:1246–72.
- [15] Goncalves J, De Moura M, De Castro P, Marques A. Interface element including point-to-surface constraints for three-dimensional problems with damage propagation. *Eng Comput* 2000;17:28–47.
- [16] Gao Y, Bower A. A simple technique for avoiding convergence problems in finite element simulations of crack nucleation and growth on cohesive interfaces. *Mod Simul Mater Sci Eng* 2004;12:453–63.
- [17] Hu N, Zemba Y, Fukunaga H, Wang H, Elmarakbi A. Stable numerical simulations of propagations of complex damages in composite structures under transverse loads. *Composites Sci Tech* 2007;67:752–65.
- [18] Riks E. An incremental approach to the solution of snapping and buckling problems. *Int J Solids Struct* 1979;15:529–51.
- [19] Gustafson PA, Waas AM. Efficient and robust traction laws for the modeling of adhesively bonded joints. In: *49th AIAA/ASME/ASCE/AHS/ASC structures, structural dynamics, and materials conference, Schaumburg, IL, AIAA-2008-1847*; 2008. p. 1–16.
- [20] De Xie, Waas AM. Discrete cohesive zone model for mixed-mode fracture using finite element analysis. *Eng Frac Mech* 2006;73:1783–96.
- [21] Livermore Software Technology Corporation, California, USA, LS-DYNA 970; 2005.
- [22] Davila C, Camanho P, de Moura M. Mixed-mode decohesion elements for analyses of progressive delamination. In: *42nd AIAA/ASME/ASCE/AHS/ASC*

- structes, structural dynamics and material conference, Washington, USA: AIAA-01-1486; 2001. p. 1–12.
- [23] Pinho S, Iannucci L, Robinson P. Formulation and implementation of decohesion elements in an explicit finite element code. *Composites A* 2006;37:778–89.
- [24] de Moura M, Gonçalves J, Marques A, de Castro P. Prediction of compressive strength of carbon-epoxy laminates containing delaminations by using a mixed-mode damage model. *Composites Struct* 2000;50:151–7.
- [25] Camanho P, Dávila C, de Moura M. Numerical simulation of mixed-mode progressive delamination in composite materials. *J Composites Mater* 2003;37(16):1415–38.
- [26] Pinho S, Camanho P, de Moura M. Numerical simulation of the crushing process of composite materials. *Int J Crashworthiness* 2004;9(3):263–76.
- [27] Morais A, Marques A, de Castro P. Estudo da aplicacao de ensaios de fractura interlaminar de modo I a laminados compositos multidireccionais. *Proceedings of the 7as jornadas de fractura, Sociedade Portuguesa de Materiais, Portugal*; 2000. p. 90–5.
- [28] Camanho P, Davila C. Mixed-mode decohesion finite elements for the simulation of delamination in composite materials. *NASA/TM-2002-211737*; 2002. p. 1–37.
- [29] Moshier M. Ram load simulation of wing skin-spar joints: new rate-dependent cohesive model. *RHAMM Technologies LLC, USA, Report No. R-05-01*; 2006.